



X-chromosome hyperactivation in mammals via nonlinear relationships between chromatin states and transcription

Citation

Yildirim, Eda, Ruslan I. Sadreyev, Stefan F. Pinter, and Jeannie T. Lee. 2013. "X-chromosome hyperactivation in mammals via nonlinear relationships between chromatin states and transcription." *Nature structural & molecular biology* 19 (1): 56-61. doi:10.1038/nsmb.2195. <http://dx.doi.org/10.1038/nsmb.2195>.

Published Version

doi:10.1038/nsmb.2195

Permanent link

<http://nrs.harvard.edu/urn-3:HUL.InstRepos:11855794>

Terms of Use

This article was downloaded from Harvard University's DASH repository, and is made available under the terms and conditions applicable to Other Posted Material, as set forth at <http://nrs.harvard.edu/urn-3:HUL.InstRepos:dash.current.terms-of-use#LAA>

Share Your Story

The Harvard community has made this article openly available. Please share how this access benefits you. [Submit a story](#).

[Accessibility](#)



Published in final edited form as:

Nat Struct Mol Biol. ; 19(1): 56–61. doi:10.1038/nsmb.2195.

X-chromosome hyperactivation in mammals via nonlinear relationships between chromatin states and transcription

Eda Yildirim^{1,2,3,¶}, Ruslan I. Sadreyev^{1,2,3,¶}, Stefan F. Pinter^{1,2,3}, and Jeannie T. Lee^{*1,2,3}

¹Howard Hughes Medical Institute, Boston, MA USA

²Department of Molecular Biology, Massachusetts General Hospital, Boston, MA USA

³Department of Genetics, Harvard Medical School Boston, MA USA

Abstract

Dosage compensation in mammals occurs at two levels. In addition to balancing X-chromosome dosage between males and females via X-inactivation, mammals also balance dosage of Xs and autosomes. It has been proposed that X-autosome equalization occurs by upregulation of X_a (active X). To investigate mechanism, we perform allele-specific ChIP-seq for chromatin epitopes and analyze RNA-seq data. The hypertranscribed X_a demonstrates enrichment of active chromatin marks relative to autosomes. We derive predictive models for relationships among POL-II, active mark densities, and gene expression, and suggest that X_a upregulation involves increased transcription initiation and elongation. Enrichment of active marks on X_a does not scale proportionally with transcription output, a disparity explained by nonlinear quantitative dependencies among active histone marks, POL-II occupancy, and transcription. Significantly, the trend of nonlinear upregulation also occurs on autosomes. Thus, X_a upregulation involves combined increases of active histone marks and POL-II occupancy, without invoking X-specific dependencies between chromatin states and transcription.

INTRODUCTION

In many organisms, sex is determined genetically by dimorphic sex chromosomes. In the XY-based system, females are homogametic (XX) and males are heterogametic (XY)^{1,2}. Current evolutionary theories suggest that sex chromosomes evolved from a pair of autosomal homologues, and acquisition of favorable male genes on the Y led to a suppression of recombination, making gradual loss of Y-chromosome material inevitable. Degeneration of the Y would have resulted in a continual series of sudden changes in gene dosage balance not only between male and female Xs, but also between X and autosomes¹. Ohno predicted that two types of dosage compensation schemes must therefore exist²⁻⁴. For mammals, the existence of X-chromosome inactivation (XCI) to silence one of the two X chromosomes in females has been known since 1961^{5,6}. This mechanism equalizes X-chromosome dosage between the sexes and depends on expression of Xist RNA⁷⁻⁹ coupled with recruitment of PRC2 complex¹⁰⁻¹². But because XCI creates another level of dosage imbalance, this one between X's and autosomes of both sexes, a secondary compensatory

*Corresponding author: lee@molbio.mgh.harvard.edu.

¶Authors contributed equally to this work.

DATABASE ACCESSION NUMBERS XXXX (will be added in proof – awaiting GEO assignment)

AUTHOR CONTRIBUTIONS E.Y. and J.T.L. designed the research; E.Y. and S.F.P. conducted ChIP-seq experiments; R.I.S. performed the bioinformatics analysis; S.F.P. performed allele-specific alignments; E.Y., R.I.S., S.F.P., and J.T.L. analyzed the data; and E.Y., R.I.S., and J.T.L. wrote the paper.

mechanism must target the active X chromosome (Xa) and double its transcription to restore genome-wide balance.

Several recent studies support the idea of X hyperactivation in mammals. Microarray-based gene expression profiling of mammalian tissues showed that X-linked genes are expressed not at half the average autosomal dose (as would be expected if expression came from a single X) but at nearly the same dose as autosomal genes in both sexes, implying that the Xa is upregulated in both males and females^{13,14}. These conclusions have been challenged by analysis of RNA-Seq data, which showed that the expression average of X-linked genes was approximately half that of the autosomal average¹⁵. A more recent study, however, indicates that this interpretation was confounded by inclusion of silent genes on the X¹⁶.

Here, we take an alternate approach to address whether and how dosage compensation occurs between X and autosomes by investigating chromatin signatures on a genome-wide scale. We carry out allele-specific chromatin immunoprecipitation with deep sequencing (ChIP-seq) for RNA polymerase II (POL-II) and activate chromatin marks and, through a combined analysis with RNA-seq data, we find that Xa upregulation indeed occurs. The data suggest that Xa upregulation occurs at the level of both transcription initiation and elongation and point to nonlinear quantitative dependencies among active histone marks, POL-II occupancies, and transcription output which are not X-specific and are part of a genome-wide mechanism for quantitative control of gene expression.

RESULTS

Confirmation of Xa upregulation

To address how X-linked transcription compares to autosomal transcription in the female soma and whether the differences, if any, could be explained by chromatin mechanisms, we first compared average gene expression of all X-linked and autosomal genes using previously published RNA-seq data from a mouse female fibroblast cell line¹⁷. We calculated gene expression levels as FPKM values (fragments per kilobase per million) for non-overlapping RefSeq mouse genes using TopHat and Cufflinks methods, and found that the total FPKM averages of haploid X and autosomal genes differed only by 22%. This conclusion is consistent with the argument that Xa-hyperactivation does not occur¹⁵.

However, the X-chromosome may harbor more silent genes than autosomes. Reasoning that this difference could confound measurements of average transcriptional output, we categorized genes with respect to their expression status (active vs inactive) and CpG content (high vs low) at the promoters (Supplementary Fig. 1a). A natural FPKM cutoff of ~1.0 for actively expressed genes was suggested by the analyses of dependency between gene expression and POL-II densities across the gene body (Supplementary Fig. 2, see Methods). We observed that almost 57% of X-linked genes were of low CpG content at promoters (LCP) with very little to no transcription (inactive). Indeed, when analysis of the RNA-seq data was performed using only expressed genes, the X-chromosome showed 85% higher mean expression than the average haploid autosome set, with 57% difference in median values (Supplementary Table I). X-hypertranscription was apparent among both active HCP and active LCP genes (Supplementary Fig. 1b). Differences between autosomal and X-linked gene populations were highly significant (Supplementary Table I, Mann-Whitney P-values; Supplementary Fig. 1c). Thus, in agreement with previous reports^{13,14,16}, the mammalian X is dosage compensated with respect to autosomes.

Allelic ChIP-seq reveals enrichment of active histone marks and POL-II on Xa

Next, we asked whether X:A dosage compensation has a chromatin basis. Over the years, genome-wide profiles of histone marks have been generated by ChIP-on-chip or ChIP-seq.

In every case, the analysis was performed either in male cell lines^{18,19} or in female lines without the allele-specificity and sequencing depth necessary to distinguish Xa from Xi with sufficient resolution²⁰⁻²². Here, we performed high-resolution, allele-specific ChIP-seq in a clonal F1 hybrid female mouse fibroblast line that carries one haploid chromosome set of *Mus musculus* (mus) origin and a second haploid set of *Mus castaneus* (cast) origins. We examined active chromatin signatures that are associated with the transcription start site (TSS), including phospho-serine-5 RNA polymerase II (POL-II-S5P) and trimethylated histone H3 at lysine 4 (H3K4me3), both of which are associated with transcription initiation; we also examined signatures associated with transcription elongation through the gene body, including phospho-serine-2 POL-II (POL-II-S2P) and trimethylated H3 at lysine 36 (H3K36me3)^{23,24}. By using paired-end sequencing, we could uniquely align 83-93% of the 17-28 million read-pairs to the genome, yielding 16.5-21.9 million uniquely aligned reads per epitope (Supplementary Table II).

With ~22 million SNP and ~1 million insertion/deletion differences between mus and cast genomes²⁵, ~35% of all read-paired could be assigned to specific alleles. Analysis of monoallelically expressed loci, including the *Zim1/Peg3* imprinted domain (Fig. 1a and data not shown), confirmed the allele-specific output of the ChIP-seq. As expected, active marks were found on the paternally expressed *Peg3* allele (cast) and the maternally expressed *Zim1* allele (mus). Elsewhere in the genome, active marks were evenly distributed between autosomal homologues, as expected (Fig. 1b). By contrast, on the X-chromosome, active marks were predominantly on X^{cast} (Xa), consistent with occurrence of XCI.

To determine whether Xa-hypertranscription is reflected in enrichment of active chromatin marks, we compared coverages on X^{cast} (Xa) with those on autosomes of *M. castaneus* origin. When we calculated medians for coverage densities on active genes, Xa showed 31% more POL-II-S5P and 24% more H3K4me3 coverage around the TSS; Xa also showed 20% more POL-II-S2P and 9% H3K36me3 coverage on the gene bodies (Fig. 2; Supplementary Table I). The enrichments were statistically significant in each category (Supplementary Table I), except for POL-II-S2P and H3K36me3 on LCP active genes, presumably due to smaller sample of LCP active genes on the Xa (n=72). Moreover, distributions of density values for all marks followed a similar shape (Fig. 2), suggesting that enrichment of Xa marks was global and could not be attributed to a distinct subset with exceptionally high coverage.

Nonlinear dependencies between active chromatin marks and transcription output

Interestingly, the enrichment of POL-II and active histone marks on Xa relative to autosomes was not proportional to the nearly 2-fold transcriptional upregulation on Xa (Fig. 2; Supplementary Table I). Indeed, the degree of epitope enrichment was much less than 2-fold. To explain this disparity, we compared POL-II and histone mark densities against transcription output genome-wide. Plotting POL-II-S2P against FPKM (transcription) values revealed a good correlation between gene expression and the elongating form of POL-II, as expected. It also demonstrated a natural separation of active genes from inactive ones (Supplementary Fig. 2: dotted horizontal line, FPKM cutoff of ~1.0) regardless of gene category (HCP, LCP, all genes). Therefore, in subsequent analyses, we used active genes of all three categories to investigate the relationship between chromatin epitope and transcription output.

The relationship between transcription output and chromatin epitopes is shown by scatterplots and point densities for Xa (black line contours) and autosomal (color contours) genes in pairwise comparisons between expression and various chromatin epitopes (Fig. 3 and Supplementary Fig. 3-4). For active HCP *M. castaneus* alleles, we found pronounced dependencies between gene expression and POL-II-S5P, POL-II-S2P and active histone

marks, regardless of whether they were X-linked or autosomal (Fig. 3a-d). Similar strong dependencies were observed between POL-II-S5P and H3K4me3 densities, and between POL-II-S2P and H3K36me3 densities (Fig. 3e-h). Similar trends were also found in the populations of all active (HCP+LCP) and active LCP genes (Supplementary Fig. 3-4). These data showed that Xa and autosomal genes are subject to similar quantitative relationships between active chromatin marks/POL-II and transcription output.

These dependencies have several universal features that might provide general insight into the mechanism of Xa upregulation. First, the relationships showed monotonic trends: Increases in POL-II or active histone marks densities were accompanied by corresponding average increases in gene expression. Second, the relationship was nonlinear, as an increase in the input variable (e.g., POL-II-S5P or H3K4me3) resulted in a much higher increase in the readout (e.g., expression). The relationship could be linearized by using log-log scale transformation, which suggested a power-law relationship. This type of dependency is consistent with previously published analysis of correlations between expression and histone mark densities at promoters²⁶. The only exceptions were H3K36me3 comparisons against all other epitopes. For both Xa and autosomal genes, a log scale transformation better linearized the trend for H3K36me3 (Fig. 3f,h and Supplementary Fig. 3-4), implying that relatively smaller changes in H3K36me3 can produce large changes in transcription output. The overall non-linearity suggests potential collective effects in the regulation of POL-II occupancy, changes in chromatin state, and transcriptional activity. Importantly, the non-linear nature of these dependencies allows for signal amplification: For example, a 20-30% increase in POL-II density corresponds to a larger increase in gene expression (Fig. 3a,b).

Third, although Xa and autosomal genes obeyed a common trend of dependency between gene expression and active chromatin/POL-II marks, the Xa scatterplot demonstrated consistent, significant shifts along the autosomal trendline to higher positions on both x- and y-axes (Fig. 3 and Supplementary Fig. 3-4), reflecting the generally higher levels of gene expression, POL-II occupancy, and H3K4me3 and H3K36me3 deposition on Xa relative to autosomes. In comparison to autosomes, Xa genes generally showed better correlations between chromatin epitopes (Fig. 4a), possibly reflecting the generally greater Xa values. Although ranges for these variables on Xa overlapped with autosomes, there was a clear distinction between the two gene populations, consistent with the significant differences in the means/medians of epitope density coverages (Supplementary Table I, Supplementary Fig. 1c and Fig. 1b).

Taken together, these data enable us to draw several conclusions regarding Xa upregulation. The similar nonlinear trends of relationships for Xa and autosomal genes suggest that Xa upregulation might be explained by chromatin-based mechanisms that are generally used throughout the genome. On both Xa and autosomes, nonlinearity of the dependencies provide a mechanism for signal amplification. For example, Xa upregulation might be explained simply by increased density of active epigenetic marks associated with increased POL-II occupancy, rather than by Xa-specific rules governing the relationship between histone marks, POL-II, and transcription. Our data also indicate that, unlike in fruitflies where enhanced transcription elongation has been proposed to be the primary mode of Xa upregulation²⁷ the mammalian mechanism displays a strong influence of enhanced transcription initiation, as both POL-II-S5P and H3K4me3 have ~30% increased coverage at the TSS of active Xa genes. At the same time, however, mammalian Xa upregulation is also associated with ~20% increase in POL-II-S2P and ~9% increase in H3K36me3 coverages across gene bodies, implying that elongation is also facilitated on Xa. We therefore propose that Xa upregulation involves both enhanced transcription initiation and elongation that depend on increased trimethylation of H3K4 and H3K36, which amplify gene expression in a nonlinear fashion (Fig. 4b).

Xa hyperactivation is predictable without necessitating Xa-specific principles

We tested this hypothesis by deriving models of gene expression based on autosomal active mark occupancy and applying these models to Xa. The resulting predictions of X-linked gene expression showed accordance with the observed values (Pearson $r=0.71$)(Fig. 4c). Moreover, autosomal models based on any combination of marks, when applied to an individual autosome, produced the correlation between predicted and observed values similar to that of Xa (Supplementary Table III; See Methods for details). These results suggested that, firstly, quantitative relationships between active histone mark densities, POL-II occupancy, and gene expression had predictive power, consistent with the results of others²⁶. Secondly, trends observed in autosomes were remarkably predictive of X-linked gene expression. Together, these conclusions argue that Xa upregulation is governed by principles that are not unique to X but are applicable throughout the genome.

DISCUSSION

We have tested the hypothesis of Xa upregulation using a novel, unbiased approach and asked whether this arm of dosage compensation is based on chromatin mechanisms similar to those observed on autosomes. By allele-specific ChIP-seq and RNA-seq analysis, we conclude that dosage compensation of Xa does occur, in agreement with previously published studies^{13,14,16}. The inability of a separate study¹⁵ to detect Xa upregulation stems from inclusion of inactive genes. When we considered all genes regardless of expression status, the average difference was masked by unusually high fraction of silent genes (genes with low-CpG content) on the X. Earlier studies^{13,14} also included both active and inactive genes; however, microarrays have a lower dynamic range and it is likely that the analysis heavily favored highly transcribed genes.

We then focused on potential mechanisms of Xa upregulation. By analyzing the genome-wide allelic distribution of POL-II and active chromatin marks in the context of gene expression¹⁷ we found that Xa was enriched for POL-II-S5P, POL-II-S2P, H3K4me3, and H3K36me3 relative to the haploid autosome set. Scatterplots (Fig. 3 and Supplementary Fig. 3-4) showed a clear rightward and upward shift of Xa contours relative to autosomal contours, along the autosomal trendline to the higher levels of active marks and expression. However, the degree of POL-II enrichment on Xa and the coverage of active histone marks did not scale proportionally with increased transcription output from Xa. This nonlinearity enables signal amplification with small changes in chromatin structure and POL-II density. An unexpected observation was that the nonlinear dependencies applied to autosomes and X alike, as suggested by all pairwise plots (Fig. 3 and Supplementary Fig. 3-4) and by the quality of predicting Xa genes based on the autosome-based models (Fig. 4c and Supplementary Table III). The similar quantitative relationships suggest that chromatin-based processes governing Xa upregulation are used genome-wide, and that dosage compensation of Xa and autosomes do not require X-specific principles to bring about the ~2-fold upregulation. Importantly, while the non-linear power laws apply to both Xa and autosomes, we do not exclude the possibility that Xa-specific factors are required to initiate the chromatin-based enhancement. Such factors could target Xa to a special compartment or lead to association with nuclear pore factors, as has been suggested for *Drosophila melanogaster*²⁸.

Our data imply similarities and differences with Xa upregulation in the fruitfly. In *D. melanogaster*, the X-chromosome dosage between XX and XY individuals is equalized by hypertranscription of the single male X-chromosome²⁹⁻³¹. With this mechanism, the fly compensates for differences between X and autosomal gene dosage at the same time it achieves male-to-female X-chromosome balance. This process requires cooperation between MOF histone acetyltransferase³², MSL complexes³³⁻³⁵, and the long noncoding RNA, roX1

and roX2^{36,37}. Together, they bring about precise chromatin change leading to ~2-fold upregulation of the male X^{27,38-45}. An alternative mechanism proposes less dependency on MSL-driven hyperactivation and more on the genome's inherent ability to correct for dosage imbalances – via the so-called “inverse effect”^{32,46}. This mechanism may also operate in mammalian Xa upregulation.

X hyperactivation in the fruitfly has been proposed to be achieved primarily through enhanced transcription elongation^{27,38,43-45}. In our system, differences in distributions of POL-II-S5P, POL-II-S2P, H3K4me3, and H3K6me3 argue that Xa upregulation is controlled through transcription initiation, but enhancement of elongation is also a strong possibility. While POL-II-S5P and H3K4me3 coverages increase ~30% at the TSS of Xa genes, POL-II-S2P and H3K36me3 coverages also increase ~20% and ~9%, respectively, across gene bodies. In conclusion, we favor a model in which Xa upregulation is effected by both enhanced transcription initiation and elongation via nonlinear dynamics. Future studies will focus on whether and how Xa-specific factors might be involved in initiating hypertranscription through the chromatin-based mechanisms identified herein.

METHODS

Cell line

To generate EY.T4 clonal hybrid cell line, female mice of *Mus musculus* (129S1) and male mice of *Mus castaneus* (CAST/EiJ) origins were crossed, F1 embryos were collected at day 13.5 and mouse embryonic fibroblasts (MEFs) were prepared using female embryos. MEFs were later immortalized by SV-40 T-antigen⁴⁷ subcloned by limiting dilution, and the chromosome content of each subclone was screened by DNA FISH using chromosome paints and RNA FISH using *Xist* RNA probe. In this clone, Xi was of *Mus musculus* and Xa was of *Mus castaneus* origins as determined by allele-specific RT-PCR using primers against *Xist* locus.

Chromatin immunoprecipitation (ChIP)

ChIP was performed as described⁴⁸ using 2×10^6 cells and 5-10 μg of antibodies per reaction. Antibodies used were as follows: H3K36me3 (ab9050, Abcam), H3K4me3 (ab8580, Abcam), POL-II-S5P (ab5131, Abcam) and POL-II-S2P (ab5095, Abcam) and IgG rabbit serum (I8140, Sigma). ChIP [DNA] was quantitated using Quant-iT Picogreen dsDNA Assay kit (Invitrogen). ChIP products for H3K4me3 and H3K36me3 were verified by PCR using primers against *c-fos* and *c-jun* genes.

ChIP library preparation and sequencing

Paired-end Solexa ChIP libraries were prepared as described in Illumina ChIP sequencing manual with minor modifications and using NEB Next DNA sample prep reagent Set 1 (E6000S) (NEB). Input DNA was used as a control and for normalization. Modifications to the Illumina protocol were: 1-30 ng of ChIP products were used as template, 2-paired-end adapters were ligated to end-repaired and A-tailed DNA using T4 DNA ligase (NEB) for 2 hours at 16°C, and 2-Phusion polymerase in GC buffer (Finzyme) was used instead of Phusion polymerase in HF buffer. DNA products were purified with QIAquick spin columns (Qiagen). Concentration, size distribution (400-500bp), and purity of libraries were assessed on DNA1000 Bioanalyzer chip (Agilent). Genome Analyzer II (Illumina) was used to perform 2x36 cycles of paired end sequencing.

Calculation of allele-specific ChIP-seq coverage

Paired-end reads (17-28 million per sample, Supplementary Table II) were aligned to two variant strain genomes (CAST/EiJ and 129S1/SvImJ) of the hybrid EY.T4 cell line. The

strain genomes were reconstructed from mm9 reference using catalogued SNPs and indels²⁵. Resulting allelic differences include ~22 million SNPs and ~1 million indels, approximately one modification per 120 bp. Alignment was performed with Novoalign 2.06 (www.novocraft.com) using default parameters with modifications: -i 300 100 -t 180 -R 10 -h 180 180 -v 180., Uniquely aligned pairs with significant score difference between the two strain alignments (>10) were classified as allele-specific and assigned to the higher-scoring allele variant; otherwise they were classified as neutral. Coverage was calculated separately for allelic tracks (cast, mus) and composite track (allelic and neutral combined) based on fragments defined by paired reads (~400 bp on average), discarding duplicate fragments. Positional coverage was normalized input coverage with a pseudocount of 1 and balanced for potential inequality of total input and experiment coverages: $n_{\text{norm}} = [(n+1)/(n_i+1)] * [N_i/N]$, where n , n_i , are positional coverages and N , N_i are total genome coverages in experiment and input, respectively. For each promoter region and gene body, allelic skew was estimated as the proportion of cumulative coverages at allelic cast/mus tracks, and corresponding fractions of composite coverage were used in further analyses.

Gene set selection

To ensure unique representation of each gene and exclude alternative transcripts, mm9 RefSeq genes were grouped into single-linkage clusters by gene body overlap and the longest gene in each cluster was chosen as a representative. Promoter regions were defined as segments including +/- 3kb from annotated TSS with high- and low-CpG promoters defined by the presence of CpG islands within 1 kb from the promoter. CpG islands were identified by using EMBOSS 6.3.1⁴⁹ on unmasked mm9 genome with default parameters.

Estimation of gene expression levels

Approximately 45 million of 36-bp RNA-seq reads by Yang et al.¹⁷ (NCBI SRA accession SRA010053) were aligned to mm9 genome using TopHat⁵⁰ with default parameters, except for using arguments --no-novel-juncs and --min-isoform-fraction 0. The resulting alignments were used to calculate FPKM (fragments per kilobase per million) values using Cufflinks⁵¹ with default parameters, except for setting --min-isoform-fraction 0. To estimate expression from a single allele, autosomal expression values were divided by 2, whereas X-linked expression values were used in full, given the well-documented inactivation of one X chromosome. As a cutoff for active expression, we chose FPKM of 1.0 corresponding to the boundary between two regimes of FPKM correlation to POL-II density on a gene (Fig. S2): the absence of dependency at low values, consistent with readout fluctuations for silent genes, and positive correlation at higher values, consistent with active transcription. Choosing FPKM cutoff of 0 produced similar values.

Linear models of gene expression

Log-transformed mark densities on autosomes (POL-II on promoters and gene bodies, H3K4me3 on promoters) and untransformed H3K36me3 on gene bodies were used for training a linear regression model that predicts logarithm of gene expression. This model (full model) was applied to the coverage densities on X chromosome, and the resulting expression predictions for X-linked genes were compared to the observed values.

To compare prediction accuracy for X chromosome and for an individual autosome, we trained and tested 19 models in a chromosome-based cross-validation setting. Specifically, a model (partial model) was trained on the autosomal gene set with one autosome removed and applied separately to the removed autosome and X chromosome. Pearson correlation coefficients between predicted and observed logarithms of expression for X chromosome were compared to the distribution of Pearson R for 19 autosomes. This comparison was made for the models based on all possible combinations of marks as predictors.

Logarithmic transformation of mark densities and expression is not defined at zero. To alleviate this problem, we used two approaches. First, we added a pseudocount of 1.0 to each value x so that $\log(x+1)$ was calculated. Second, since the fraction of zero values among actively expressed genes was relatively low we tested the removal of genes with zero values from the dataset. Both approaches produced similar results.

Supplementary Material

Refer to Web version on PubMed Central for supplementary material.

Acknowledgments

We are thankful to members of Lee laboratory for valuable discussions and to B. Chapman, M. Borowsky and T. Ohsumi of the Bioinformatics Core Facility (MGH, Molecular Biology Dept) for their suggestions for ChIP-Seq analysis. This work was supported by the MGH ECOR Medical Discovery Fund (E.Y.), DFG (S.F.P.), and the National Institutes of Health (RO1-GM090278, J.T.L.). J.T.L. is an investigator of the Howard Hughes Medical Institute.

REFERENECES

1. Charlesworth B. The evolution of chromosomal sex determination and dosage compensation. *Current biology* : CB. 1996; 6:149–62. [PubMed: 8673462]
2. Ohno S. More about the mammalian X chromosome. *Lancet*. 1962; 2:152–3. [PubMed: 14481406]
3. Ohno S. A phylogenetic view of the X-chromosome in man. *Annales de genétique*. 1965; 8:3–8. [PubMed: 5320583]
4. Ohno, S. *Sex Chromosomes and Sex Linked Genes*. Springer Verlag; Berlin: 1967.
5. Lyon MF. Gene action in the X-chromosome of the mouse (*Mus musculus* L.). *Nature*. 1961; 190:372–3. [PubMed: 13764598]
6. Lyon MF. Possible mechanisms of X chromosome inactivation. *Nat New Biol*. 1971; 232:229–32. [PubMed: 5286191]
7. Penny GD, Kay GF, Sheardown SA, Rastan S, Brockdorff N. Requirement for Xist in X chromosome inactivation. *Nature*. 1996; 379:131–7. [PubMed: 8538762]
8. Brockdorff N, et al. High-density molecular map of the central span of the mouse X chromosome. *Genomics*. 1991; 10:17–22. [PubMed: 1675191]
9. Brown M, et al. A recombinant murine retrovirus for simian virus 40 large T cDNA transforms mouse fibroblasts to anchorage-independent growth. *Journal of virology*. 1986; 60:290–3. [PubMed: 3018293]
10. Silva J, et al. Establishment of histone h3 methylation on the inactive X chromosome requires transient recruitment of Eed-Enx1 polycomb group complexes. *Developmental cell*. 2003; 4:481–95. [PubMed: 12689588]
11. Plath K, et al. Role of histone H3 lysine 27 methylation in X inactivation. *Science*. 2003; 300:131–5. [PubMed: 12649488]
12. Zhao J, Sun BK, Erwin JA, Song JJ, Lee JT. Polycomb proteins targeted by a short repeat RNA to the mouse X chromosome. *Science*. 2008; 322:750–6. [PubMed: 18974356]
13. Lin H, et al. Dosage compensation in the mouse balances up-regulation and silencing of X-linked genes. *PLoS biology*. 2007; 5:e326. [PubMed: 18076287]
14. Nguyen DK, Disteche CM. Dosage compensation of the active X chromosome in mammals. *Nature genetics*. 2006; 38:47–53. [PubMed: 16341221]
15. Xiong Y, et al. RNA sequencing shows no dosage compensation of the active X-chromosome. *Nature genetics*. 2010; 42:1043–7. [PubMed: 21102464]
16. Deng X, et al. Evidence for compensatory upregulation of expressed X-linked genes in mammals, *Caenorhabditis elegans* and *Drosophila melanogaster*. *Nature genetics*. 2011
17. Yang F, Babak T, Shendure J, Disteche CM. Global survey of escape from X inactivation by RNA-sequencing in mouse. *Genome research*. 2010; 20:614–22. [PubMed: 20363980]

18. Meissner A, et al. Genome-scale DNA methylation maps of pluripotent and differentiated cells. *Nature*. 2008; 454:766–70. [PubMed: 18600261]
19. Mikkelsen TS, et al. Dissecting direct reprogramming through integrative genomic analysis. *Nature*. 2008; 454:49–55. [PubMed: 18509334]
20. Marks H, et al. High-resolution analysis of epigenetic changes associated with X inactivation. *Genome research*. 2009; 19:1361–73. [PubMed: 19581487]
21. O'Neill LP, et al. X-linked genes in female embryonic stem cells carry an epigenetic mark prior to the onset of X inactivation. *Human molecular genetics*. 2003; 12:1783–90. [PubMed: 12874099]
22. O'Neill LP, Spotswood HT, Fernando M, Turner BM. Differential loss of histone H3 isoforms mono-, di- and tri-methylated at lysine 4 during X-inactivation in female embryonic stem cells. *Biological chemistry*. 2008; 389:365–70. [PubMed: 18225985]
23. Bernstein BE, et al. Genomic maps and comparative analysis of histone modifications in human and mouse. *Cell*. 2005; 120:169–81. [PubMed: 15680324]
24. Schneider R, et al. Histone H3 lysine 4 methylation patterns in higher eukaryotic genes. *Nature cell biology*. 2004; 6:73–7.
25. Keane TM, et al. Mouse genomic variation and its effect on phenotypes and gene regulation. *Nature*. 2011; 477:289–94. [PubMed: 21921910]
26. Karlic R, Chung HR, Lasserre J, Vlahovicek K, Vingron M. Histone modification levels are predictive for gene expression. *Proceedings of the National Academy of Sciences of the United States of America*. 2010; 107:2926–31. [PubMed: 20133639]
27. Larschan E, et al. X chromosome dosage compensation via enhanced transcriptional elongation in *Drosophila*. *Nature*. 2011; 471:115–8. [PubMed: 21368835]
28. Vaquerizas JM, et al. Nuclear pore proteins nup153 and megator define transcriptionally active regions in the *Drosophila* genome. *PLoS genetics*. 2010; 6:e1000846. [PubMed: 20174442]
29. Payer B, Lee JT. X chromosome dosage compensation: how mammals keep the balance. *Annual review of genetics*. 2008; 42:733–72.
30. Lucchesi JC, Kelly WG, Panning B. Chromatin remodeling in dosage compensation. *Annual review of genetics*. 2005; 39:615–51.
31. Cline TW, Meyer BJ. Vive la difference: males vs females in flies vs worms. *Annual review of genetics*. 1996; 30:637–702.
32. Bhadra MP, Bhadra U, Kundu J, Birchler JA. Gene expression analysis of the function of the male-specific lethal complex in *Drosophila*. *Genetics*. 2005; 169:2061–74. [PubMed: 15716510]
33. Palmer MJ, Richman R, Richter L, Kuroda MI. Sex-specific regulation of the male-specific lethal-1 dosage compensation gene in *Drosophila*. *Genes & development*. 1994; 8:698–706. [PubMed: 7926760]
34. Gu W, Szauter P, Lucchesi JC. Targeting of MOF, a putative histone acetyl transferase, to the X chromosome of *Drosophila melanogaster*. *Developmental genetics*. 1998; 22:56–64. [PubMed: 9499580]
35. Lyman LM, Copps K, Rastelli L, Kelley RL, Kuroda MI. *Drosophila* male-specific lethal-2 protein: structure/function analysis and dependence on MSL-1 for chromosome association. *Genetics*. 1997; 147:1743–53. [PubMed: 9409833]
36. Meller VH, Wu KH, Roman G, Kuroda MI, Davis RL. roX1 RNA paints the X chromosome of male *Drosophila* and is regulated by the dosage compensation system. *Cell*. 1997; 88:445–57. [PubMed: 9038336]
37. Amrein H, Axel R. Genes expressed in neurons of adult male *Drosophila*. *Cell*. 1997; 88:459–69. [PubMed: 9038337]
38. Gelbart ME, Kuroda MI. *Drosophila* dosage compensation: a complex voyage to the X chromosome. *Development*. 2009; 136:1399–410. [PubMed: 19363150]
39. Hilfiker A, Hilfiker-Kleiner D, Pannuti A, Lucchesi JC. mof, a putative acetyl transferase gene related to the Tip60 and MOZ human genes and to the SAS genes of yeast, is required for dosage compensation in *Drosophila*. *The EMBO journal*. 1997; 16:2054–60. [PubMed: 9155031]

40. Akhtar A, Becker PB. Activation of transcription through histone H4 acetylation by MOF, an acetyltransferase essential for dosage compensation in *Drosophila*. *Molecular cell*. 2000; 5:367–75. [PubMed: 10882077]
41. Smith ER, et al. The *Drosophila* MSL complex acetylates histone H4 at lysine 16, a chromatin modification linked to dosage compensation. *Molecular and cellular biology*. 2000; 20:312–8. [PubMed: 10594033]
42. Prestel M, Feller C, Straub T, Mitlohner H, Becker PB. The activation potential of MOF is constrained for dosage compensation. *Molecular cell*. 2010; 38:815–26. [PubMed: 20620953]
43. Alekseyenko AA, Larschan E, Lai WR, Park PJ, Kuroda MI. High-resolution ChIP-chip analysis reveals that the *Drosophila* MSL complex selectively identifies active genes on the male X chromosome. *Genes & development*. 2006; 20:848–57. [PubMed: 16547173]
44. Gilfillan GD, et al. Chromosome-wide gene-specific targeting of the *Drosophila* dosage compensation complex. *Genes & development*. 2006; 20:858–70. [PubMed: 16547172]
45. Legube G, McWeeney SK, Lercher MJ, Akhtar A. X-chromosome-wide profiling of MSL-1 distribution and dosage compensation in *Drosophila*. *Genes & development*. 2006; 20:871–83. [PubMed: 16547175]
46. Birchler J, et al. Re-evaluation of the function of the male specific lethal complex in *Drosophila*. *Journal of genetics and genomics = Yi chuan xue bao*. 2011; 38:327–32. [PubMed: 21867958]
47. Brown CJ, et al. Localization of the X inactivation centre on the human X chromosome in Xq13. *Nature*. 1991; 349:82–4. [PubMed: 1985270]
48. Takahashi K, Saitoh S, Yanagida M. Application of the chromatin immunoprecipitation method to identify in vivo protein-DNA associations in fission yeast. *Science's STKE : signal transduction knowledge environment*. 2000; 2000:p11.
49. Rice P, Longden I, Bleasby A. EMBOSS: the European Molecular Biology Open Software Suite. *Trends in genetics : TIG*. 2000; 16:276–7. [PubMed: 10827456]
50. Trapnell C, Pachter L, Salzberg SL. TopHat: discovering splice junctions with RNA-Seq. *Bioinformatics*. 2009; 25:1105–11. [PubMed: 19289445]
51. Trapnell C, et al. Transcript assembly and quantification by RNA-Seq reveals unannotated transcripts and isoform switching during cell differentiation. *Nature biotechnology*. 2010; 28:511–5.
52. Kim J, Lu X, Stubbs L. Zim1, a maternally expressed mouse Kruppel-type zinc-finger gene located in proximal chromosome 7. *Human molecular genetics*. 1999; 8:847–54. [PubMed: 10196374]
53. Kuroiwa Y, et al. Peg3 imprinted gene on proximal chromosome 7 encodes for a zinc finger protein. *Nature genetics*. 1996; 12:186–90. [PubMed: 8563758]

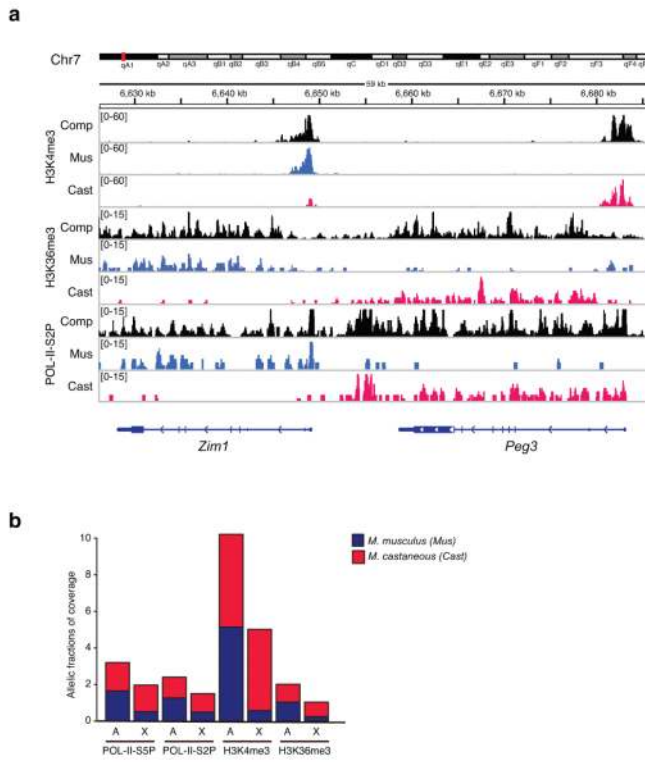


Figure 1. Allele-specific ChIP-seq

(a) Profiles for POL-II-S5P, H3K4me3, and H3K36me3 are mapped to *M. castaneus* (*cast*) or *M. musculus* (*mus*) alleles for two imprinted loci, *Zim1*⁵² and *Peg3*⁵³ on Chromosome 7. Composite tracks (comp) represent combination of *cast*, *mus* and neutral reads. Coverage values are normalized by input and are indicated on the y-axis. (b) X chromosome shows a strong allelic skew in the occupancy of active histone marks and POL-II at the TSS and across the gene body. Barplots show mean composite densities of H3K4me3, H3K36me3, POL-II-S2P and POL-II-S5P on autosomes (A) and X chromosome (X), with proportion of allelic coverage indicated by red (*cast*), and blue (*mus*) fractions. Inactive X (X^{mus}), and active X (X^{cast}).

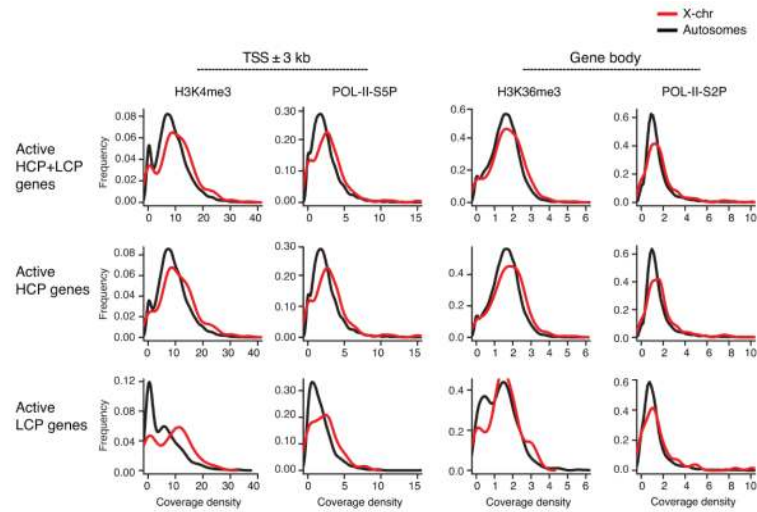


Figure 2. Distributions of coverage densities for POL-II and active histone modifications on X chromosome and autosomes

Coverage density values are shown for H3K4me3 and POL-II-S5P at the TSS and for H3K36me3 and POL-II-S2P across the gene bodies as indicated. Distributions are plotted for actively transcribed (HCP+LCP, HCP and LCP) genes. Black line, autosomal genes; red line, X-linked genes.

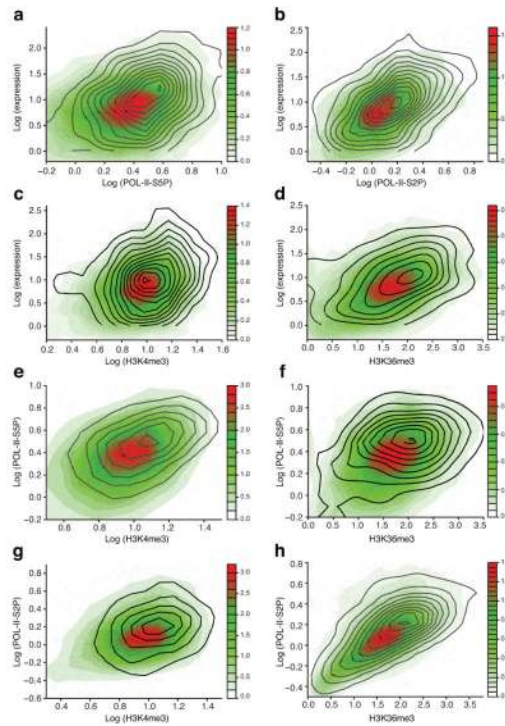


Figure 3. Relationships between levels of gene expression, POL-II, and active histone modifications

M. castaneus alleles of actively expressed autosomal HCP genes are represented as points, with point density shown by colored contour. Black line contour represents active HCP X-linked *M. castaneus* alleles (Xa). Expression, POL-II, and histone modification levels are positively correlated, the relationships are non-linear, and X-linked genes follow autosomal trends of dependency, albeit with a shift to higher values. (a,b) POL-II at the TSS (a) and across the gene body (b) vs expression (log-log scale). (c) H3K4me3 at the TSS vs expression (log-log scale). (d) H3K36me3 across the gene body vs expression (linear-log scale). (e) H3K4me3 vs POL-II at the TSS (log-log scale). (f) H3K36me3 across the gene body vs POL-II at the TSS (linear-log scale). (g) H3K4me3 at the TSS vs POL-II across the gene body (log-log scale). (h) H3K36me3 vs POL-II across the gene body (linear-log scale).

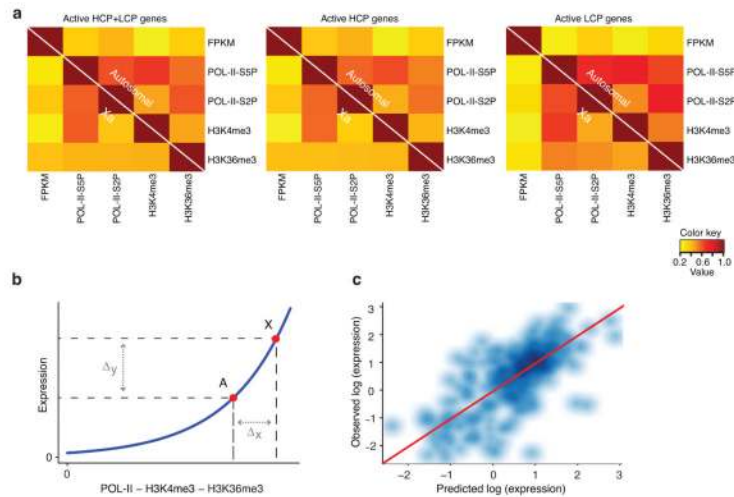


Figure 4. Autosomal relationships between active histone modifications, POL-II, and expression are predictive of X-linked gene expression

(a) Actively expressed X-linked and autosomal genes show similar patterns of correlation between the levels of active marks and expression. Pearson correlation coefficients between the levels of all marks and expression (FPKM) are shown as heatmaps for actively expressed (HCP+LCP, HCP, and LCP) genes. In each plot, autosomal and X chromosome correlations are shown above and below diagonal, respectively. (b) Active X chromosome loci (X) and the corresponding set of autosomal loci (A) show similar non-linear relationship between active marks and expression (blue curve), which produces a large average expression change in response to smaller changes in the mark occupancy (schematic). (c) Scatterplot of X-linked gene expression values predicted from autosome-based full linear model vs observed X-linked expression (log-log scale). Shades of blue indicate point density. Identity line $y=x$ is shown in red.